CHEMSUSCHEM

DOI: 10.1002/cssc.200800215

Carbon-Supported, Selenium-Modified Ruthenium–Molybdenum Catalysts for Oxygen Reduction in Acidic Media

Maxime J.-F. Guinel,[b] Arman Bonakdarpour,[a] Biao Wang,[a, c] Panakkattu K. Babu,[a] Frank Ernst,[b] Nagappan Ramaswamy,[d] Sanjeev Mukerjee,[d] and Andrzej Wieckowski*[a]

The stability and oxygen reduction activity of two carbon-supported catalyst materials are reported. The catalysts, Se/Ru and Se/(Ru–Mo), were prepared by using a chemical reduction method. The catalyst nanoparticles were evenly dispersed onto globular amorphous carbon supports, and their average size was ca. 2.4 nm. Thermal treatment at 500 °C for 2 h in an inert argon atmosphere resulted in coarsening of the nanoparticles, and also in some decrease of their activity. A gradual reduction of activity was also observed for Se/Ru during potential-cycle experiments. However, the incorporation of small amounts of Mo into the Se/Ru catalysts considerably improved the stability of the catalyst against dissolution. The Mo-containing samples showed excellent oxygen reduction activities even after cycling the potential 1000 times between 0.7 and 0.9 V. Furthermore, they showed excellent fuel-cell behavior. The performance of the Se/Ru catalysts is greatly improved by the addition of small amounts of elemental Mo. Possible mechanisms responsible for the improvement of the activity are discussed.

Introduction

Direct methanol fuel cells (DMFCs) have attracted considerable interest for application in vehicles and as alternative power sources for portable devices.[1] The commercialization of DMFCs, however, has been restrained because of their prohibitive cost and relatively poor performance.[2–4] Further progress in DMFC technology is driven by the development of improved materials for both fuel-cell anodes and cathodes as well as improved membrane electrolytes. In particular, new cathode catalysts must be developed in order to replace the traditionally used Pt alloys and pure Pt, which are too expensive and show relatively poor performance.[5] Cathodes with Pt catalysts also suffer from performance degradation due to some methanol diffusing from the anode to the cathode through the polymer membrane.[6,7] Therefore, alternative Pt-free and methanol-tolerant cathode catalyst materials need to be developed; these would ideally show high activities, performance stability, and long lifetimes for the oxygen reduction.

As originally reported by Alonso-Vante and co-workers,[8,9] Ru-based chalcogenides (Ru_xSe_y) are excellent oxygen reduction reaction (ORR) cathode catalysts. These clusterlike Ru_xSe_y materials were synthesized from Ru carbonyl ($Ru_3(CO)_{12}$) using elemental Se in organic media,[8,10] and they were shown to reduce O_2 to H_2O predominantly via a four-electron process, with less than 5% of H_2O_2 produced. Other Se/Ru-based catalysts for oxygen reduction have been reported.[11–13] Transition metals, such as Fe,[14] W,[15] and Mo,[16] were incorporated into the Ru_xSe_y-type materials. Except for the case of the Mo additive,[16] the ORR activity was not markedly improved. The effect of transition metals on the chalcogenide catalyst activity still remains a major focus of study. More recently, commercially available Ru nanoparticles[17] and synthesized carbon-supported Ru nanoparticles[18] were used as the catalyst precursors. These novel catalysts displayed ORR activities on par with the clusterlike materials.

To further enhance the catalytic activity and improve the stability, we synthesized carbon-supported Ru-based chalcogenide catalysts of the Se/Ru/C type by an aqueous chemical reduction method.[19,31] The catalysts produced in this manner showed high ORR activities compared to other Ru-based chalcogenide catalysts. Furthermore, we found that incorporating small amounts of elemental Mo into these catalysts considerably increased their stability. Herein, we report on the synthesis; detailed structural characterization, using mostly transmission electron microscopy; elemental analysis; and electrochemical measurements of the carbon-supported chalcogenide catalysts.

[a] Dr. A. Bonakdarpour, Dr. B. Wang, Dr. P. K. Babu, Prof. A. Wieckowski
Department of Chemistry
University of Illinois at Urbana–Champaign
600 South Mathews Avenue, Urbana, IL 61801 (USA)
Fax: (+1) 217-244-8068
E-mail: andrzej@scs.uiuc.edu

[b] Dr. M. J.-F. Guinel, Prof. F. Ernst
Department of Materials Science and Engineering
Case Western Reserve University
10900 Euclid Avenue, Cleveland, OH 44106-7204 (USA)

[c] Dr. B. Wang
College of Material Science and Engineering
Donghua University
1882 West Yan-an Road, Shanghai, 200051 (PR China)

[d] Dr. N. Ramaswamy, Prof. S. Mukerjee
Department of Chemistry and Chemical Biology
Northeastern University
360 Huntington Avenue, Boston, MA 02115 (USA)

Results and Discussion

X-ray diffraction (XRD) patterns of the Se/Ru/C and Se/(Ru–Mo)/C catalyst materials are shown in Figure 1 a and b, respectively. The XRD pattern of the heat-treated carbon substrate

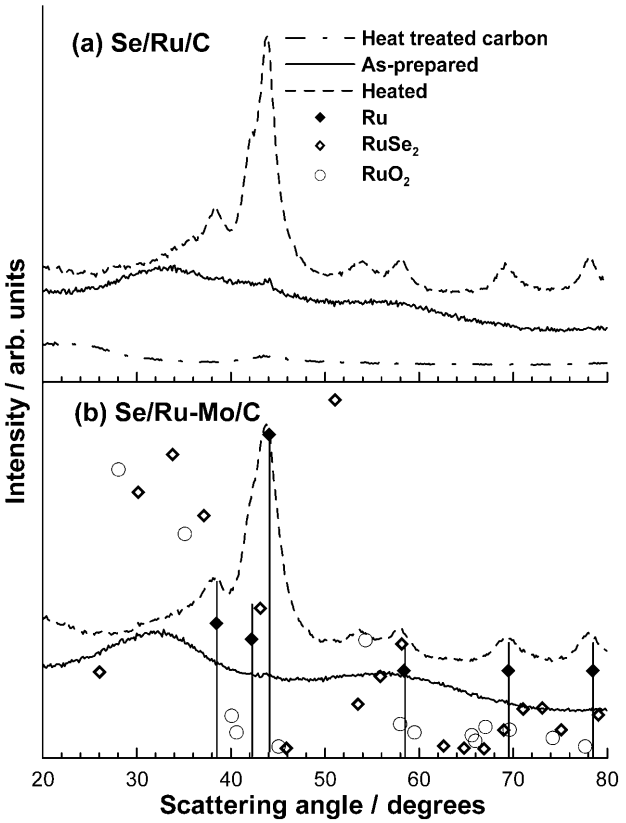

Figure 1. XRD patterns of as-prepared and heat-treated samples of a) Se/Ru/C and b) Se/(Ru–Mo)/C. The corresponding reflection peaks from Ru, RuO_2, and $RuSe_2$ are also shown.

(Figure 1 a) shows broad scattering around 21° and 43°. For the "as prepared" (i.e., non-heat-treated) Se/Ru/C and Se/(Ru–Mo)/C materials, the presence of very broad Bragg peaks indicates nanocrystalline (2 nm or smaller) grains, which may consist of $RuSe_2$ or RuO_2. These diffraction patterns show that the aqueous chemical reduction is able to produce nanoparticles. Once heat-treated, both Se/Ru/C and Se/(Ru–Mo)/C crystallize in a Ru-like hexagonal structure. The crystalline phase dominates the XRD patterns; however, nanometer-sized $RuSe_2$ and/or RuO_2 could still be present. The average grain size, estimated from the broadening of the Bragg peaks after heat treatment, is ca. 8 nm.

X-ray energy-dispersive spectroscopy (XEDS) measurements were acquired either from large volumes or in spot mode. The "overall" measurements were carried out to determine the global composition of the samples (the electron beam was scanned in a window of at least 1 μm^2). The elemental compositions of individual nanoparticles could be determined by using the spot mode. The global composition was obtained by averaging from at least 3 different areas, while local compositions were determined from at least 10 particles. The measured global compositions were in agreement with the nominal compositions of the catalysts. The mean ratio of Ru to Se was found to be 1.7 ± 0.3, which is very close to the mass of the starting materials used. Spot-mode measurements, in contrast, showed significant scatter. The mean value for the Se fraction was found to be (30 ± 5) at%. This value is, within the uncertainty levels, in agreement with the Se level observed in "overall" mode (which mainly probes the carbon support between the nanoparticles), indicating that the Se resides within the catalyst nanoparticles and is not dispersed across the carbon support.

A thermal treatment is considered an effective way to improve the ORR activity of carbon-supported Ru-based catalysts.[16] For example,[20] heating the carbon-supported Ru_xSe_y catalysts at 900 °C increased their ORR activity despite the mean size of the nanoparticles reaching 10 nm.

The morphology of the as-synthesized catalyst is shown in Figure 2. All samples were found to agglomerate heavily into brittle conglomerates, with lumps sometimes approaching

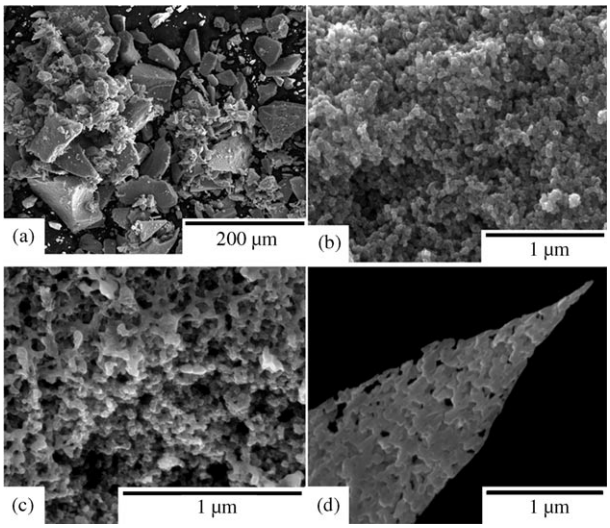

Figure 2. Scanning electron microscopy images, showing the morphology of the materials. a) In all cases, the nanoparticles tended to agglomerate heavily into large lumps. The material is shown b) before and c) after heat treatment. d) Cross-section, obtained by focused ion beam milling of one large agglomerate of a heat-treated sample.

sizes of up to a millimeter. However, these broke down easily when dispersed and sonicated in a solvent such as methanol. The heat treatment (500 °C, 2 h, Ar) not only improved the catalytic performances but also tended to result in coalescence of the catalytic materials themselves, as illustrated in Figure 2 b and c. It was confirmed that the large agglomerates pictured in Figure 2 a were actual conglomerates of much-smaller nanoparticles; several cross-sections deep into these agglomerates were made by using focused ion beam (FIB) milling, and a typical scanning electron microscopy (SEM) image is shown in Figure 2 d. Note that most of the material consisted of the globular amorphous carbon support and that the phases containing

Ru, Se, and Mo were much smaller and decorated its surface. The nanoparticles were less than 10 nm in size, as shown later in the transmission electron microscopy (TEM) images, and could therefore not be resolved using our SEM instrument.

Numerous XEDS measurements were recorded, and the materials were found to consist only of Ru, Se, Mo, and C. No impurities were detected. Moreover, the heat treatment had no effect on the elemental composition of the samples. Ru, Se, and Mo were present in concentrations of approximately 56, 40, and 3 at%, respectively. XEDS spectra were also collected by using the transmission electron microscope, and the obtained results were in accordance with those collected by using the scanning electron microscope. This shows that the sampling technique used for the TEM analyses does not alter the composition of the samples. However, we note that when an XEDS spectrum is collected by SEM the surface of these agglomerates is sampled, while when the spectrum is recorded by TEM it is more likely that the material originating from the bulk of the agglomerates is probed because they are dispersed; this may explain the slight variations in elemental composition between the two measurements. Two XEDS spectra, of non-heat-treated and heat-treated Se/(Ru–Mo)/C samples, respectively, are shown in Figure 3a and b. The magnification was set at a low value so that the collected signal would originate from a large volume of material and be more uniform and representative of the full sample. The peaks for Ru (L_α ~ 2.56 keV, L_β ~ 2.71 keV), Se (L_α ~ 1.39 keV), and Mo (L_α ~ 2.29 keV, L_β ~ 2.41 keV) are indicated on the figures. The elemental compositions were found to be similar for both samples: approximately 67–70 at% Ru, 27–31 at% Se, and 2 at% Mo. This clearly indicates that heat-treatment would only be responsible for a rearrangement of the elements initially present in the material.

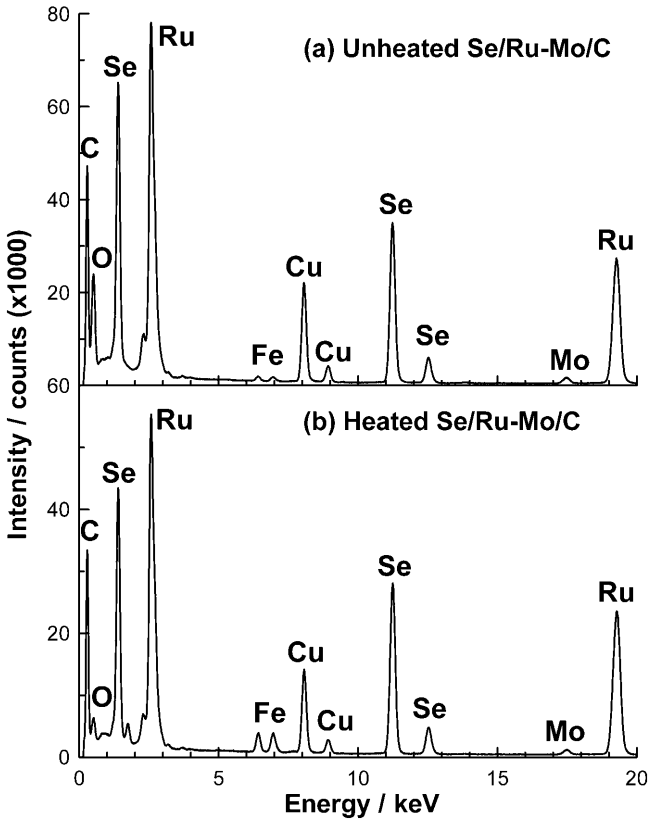

Figure 3. XEDS spectra of a) non-heat-treated and b) heat-treated Se/Ru–Mo/C samples, recorded by TEM. The Cu and Fe peaks originate from the copper support grid and the pole pieces, respectively.

Figure 4 shows electron diffraction patterns of the as-prepared and heat-treated Se/(Ru–Mo)/C samples. The as-prepared Se/(Ru–Mo)/C material, Figure 4a, showed broad rings,

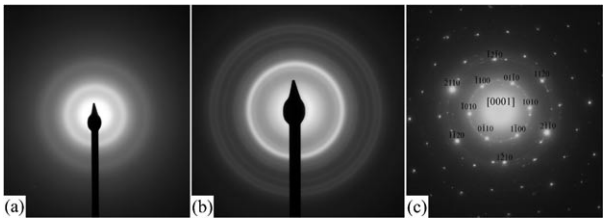

Figure 4. Electron diffraction patterns obtained from a) non-heat-treated and b,c) heat-treated Se/(Ru–Mo)/C samples. Heat treatment apparently results in ordering of the elements present in the material. Samples which have not undergone heat treatment appear as mostly amorphous, as shown in (a). The polycrystalline ring pattern shown in (b) could be indexed to hexagonal Ru, and sometimes it was possible to record patterns of Ru nanoparticles on low-index zone axes, as illustrated in (c); in this case, indexed to hexagonal Ru on the [0001] zone axis. Additional spots or rings from neighboring particles are also present.

indicating an amorphous-like structure. After heat treatment, however, the width of the diffuse rings in the diffraction pattern decreased and became more characteristic of a polycrystalline material, indicating crystallization of the catalyst metals. Figure 4b shows a ring pattern typical of a polycrystalline material, which could be indexed to the hexagonal close-packed (HCP) structure of Ru. Figure 4c shows the single-crystal diffraction pattern obtained from a grain, and is indexed to the hexagonal lattice of Ru (space group $P6_3/mmc$) on the [0001] zone axis, with lattice parameters $a = 0.275$ nm and $c = 0.428$ nm. These electron diffraction patterns are in agreement with the powder XRD data shown in Figure 1.

Figure 5 shows a typical high-resolution (HR)TEM image obtained from the heat-treated sample. Three Ru particles are pointed out, including one faceted on the $\{\bar{1}100\}$ planes and viewed along the $[\bar{2}113]$ direction. The grains are typically ca. 8 to 10 nm in size. Single grains were generally agglomerated, however, individual crystallites could also be observed, as illustrated in the inset of Figure 5. This particle is viewed along its $[0\bar{1}11]$ zone axis, and also measures approximately 8 nm in diameter, but is not faceted.

A more careful examination of the heat-treated samples revealed the presence of additional phases in some minor quantities, more precisely, $MoSe_2$, $RuSe_2$, and Se. This is clearly illustrated in Figure 6. $MoSe_2$, like Ru, crystallizes in a hexagonal unit cell with cell parameters $a = 0.329$ nm and $c = 1.293$ nm. $RuSe_2$ is cubic with the space group Pa-3 and a lattice parameter $a = 0.593$ nm. The Se crystal shown in Figure 6e is rhombohedral with the space group R-3 and $a = 1.141$ nm and $c =$

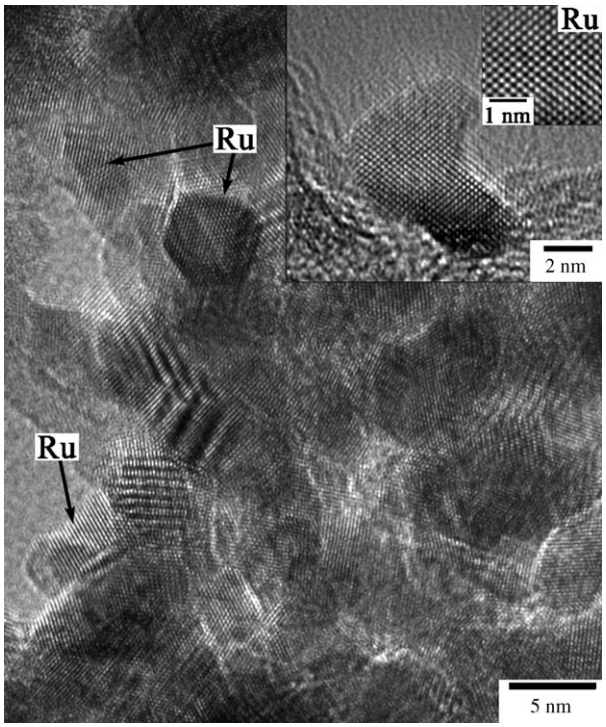

Figure 5. HRTEM image of a heat-treated sample, consisting of mostly Ru nanoparticles. The Ru particles were often found to agglomerate and sometimes facet along specific directions; one such hexagonal particle is shown in this image and is facetted on its (0001) and ($\bar{1}$100) planes and is viewed along the [$\bar{2}$113] direction. The inset shows an example of another type of hexagonal Ru nanoparticles that were encountered in the samples, which were isolated and attached on the globular amorphous carbon support. In this case, the Ru particle is viewed along its [0$\bar{1}$11] zone axis.

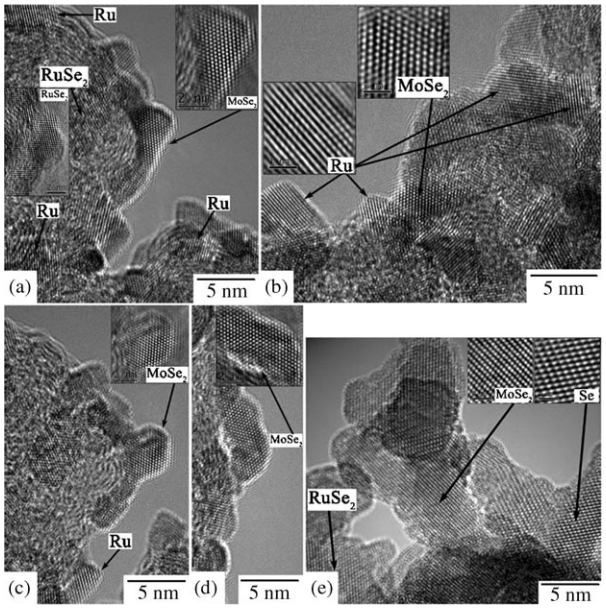

Figure 6. a–e) HRTEM images obtained from heat-treated samples. The samples consist mostly of Ru nanoparticles with hexagonal crystal structure, but this demonstrates that the samples do actually contain additional phases, including $MoSe_2$, $RuSe_2$, and Se.

0.444 nm. These phases are present in such small quantities that they could not be detected by using either powder XRD or electron diffraction. The samples did not show continuous amorphous films of any of the Se- or Ru-containing phases (e.g., SeO_2). The incorporation of a small amount of Mo (about 2 to 3 at%) in the Ru/Se samples was found to considerably improve the stability of the catalyst materials against dissolution under potential cycling conditions, however, at this time further work is required to understand the role of Mo as a stabilizing agent. Zehl et al. have hypothesized a structural model for Ru/Se particles assuming firmly interacting Se that only partially decorates the surface of primary Ru core particles.[21] This is not what was observed in any of the samples that were examined in this study.

The average half-wave potential, $E_{1/2}$, of the heat-treated Se/Ru/C samples was 0.74 V, which represents a 20 mV decrease compared to the original Se/Ru/C sample (Figure 7). The degradation may be caused by the loss of some Se upon heating, which weakens the protection by Se against oxidation of metallic Ru.[17]

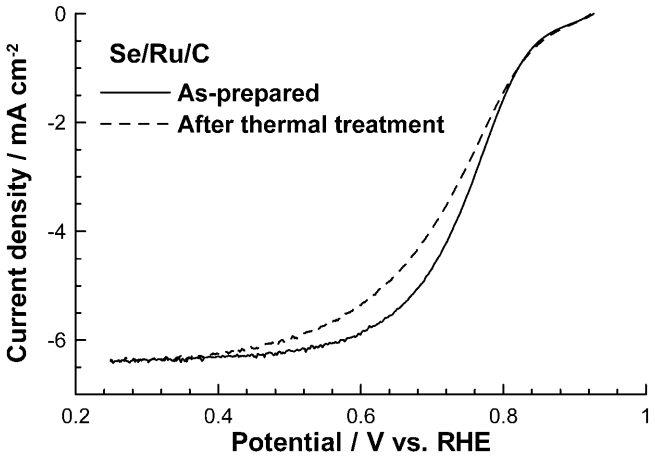

Figure 7. ORR hydrodynamic voltammograms using the as-prepared and heat-treated Se/Ru/C nanoparticles. The measurements were carried out in a O_2-saturated 0.1 M H_2SO_4 solution at 20 mV s^{-1} and 1600 rpm.

The exceptional methanol tolerance of chalcogenide Se/Ru catalytic materials is well-established.[9,17,22,23] However, the stability of the Ru-based chalcogenide catalysts is an issue that as yet deserves consideration.[24,25] In this work, we used a laboratory test to check the stability of the catalysts by applying voltammetric potential sweeps in O_2-saturated 0.1 M H_2SO_4 solutions. The potential range was chosen from 0.7 to 0.9 V (at a rate of 20 mV s^{-1}), that is, around the potential for practical ORR electrodes.[20] Figure 8a shows a 70 mV loss in $E_{1/2}$ after 1000 cycles. Potential cycling leads to a loss of Se and, hence, loss of activity.[17,26]

The Se/(Ru–Mo)/C showed an activity ($E_{1/2}$ = 0.76 V) similar to that of Se/Ru/C (Figure 8b). As can be seen from the figure, the catalytic activity of Se/(Ru–Mo)/C measured after potential cycling showed almost no degradation in $E_{1/2}$ over the cycling

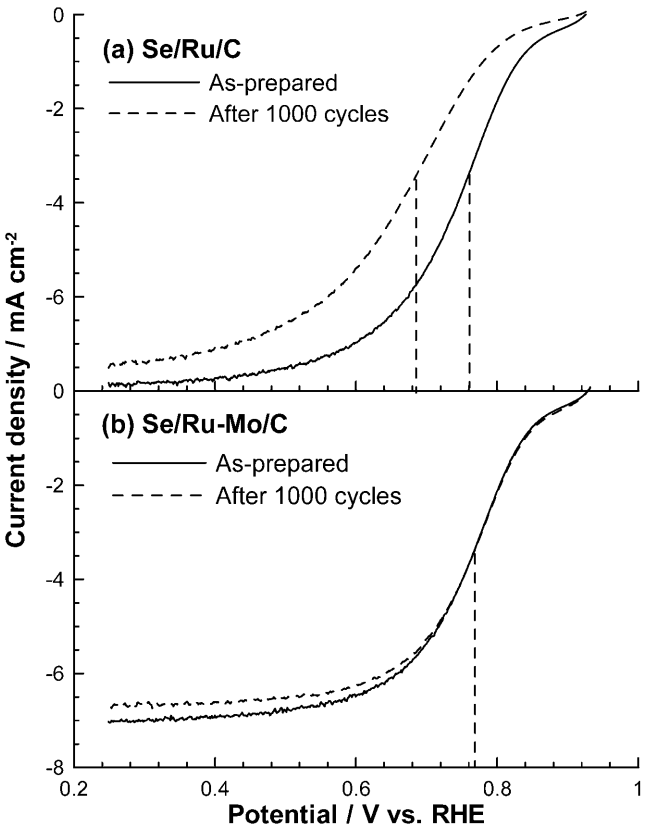

Figure 8. ORR hydrodynamic voltammograms with a) Se/Ru/C and b) Se/(Ru–Mo)/C catalysts before and after 1000 potential cycles. The potential cycles were taken from 0.7 to 0.9 V in O_2-saturated 0.1 M H_2SO_4 solution at 20 V s^{-1} and 1600 rpm.

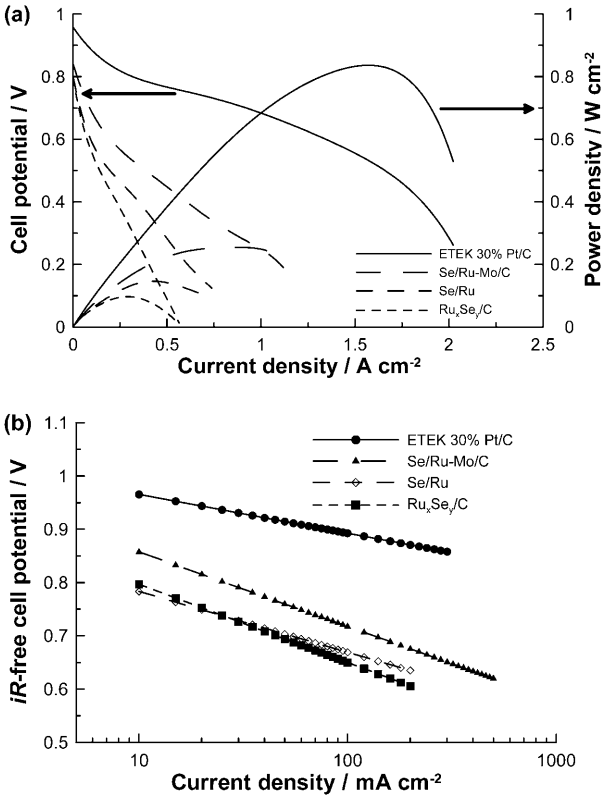

Figure 9. a) Steady-state polarization data measured in a polymer electrolyte fuel cell using single-cell mode with a built-in RHE at the anode side for H_2/O_2. b) Corresponding Tafel plots, showing the kinetic region of the polarization measurements.

period, which indicates that the presence of Mo could improve the stability of Se in the catalyst particles. The Se in the catalyst could be more stable owing to an interaction with Mo, and might therefore better protect Ru against oxidation. This occurs despite the small amount of Mo present (about 2 to 3 at%). Further work is required to understand the role of Mo as a stabilizing agent under the potential-cycling conditions.

Steady-state polarization data, shown in Figure 9a and b, correspond to a representative single fuel-cell test at 80 °C with H_2/O_2, 0.4 MPa back pressure (anode and cathode), and 100% relative humidity. The measurements showed very good activity for the chalcogenide cathode electrodes (except for Pt) and are the highest reported steady-state performances to date.[27–29] Addition of about 2–3 at% Mo resulted in a three-fold increase of the steady-state polarization of Se/Ru. Under normal fuel-cell operating conditions, that is, at 0.6 V, remarkable power density improvements are obtained. This indicates a synergistic effect of Mo on the ORR active sites on the Ru nanoparticles, in good agreement with the rotating disk electrode (RDE) data reported above. Contrary to what was reported by Christensen et al.,[27] where improvement in only the mass transport region of the polarization curve was observed, these results indicate a beneficial effect of Mo in all regions of the curve (activation, ohmic, and mass transport). Note, however, that the results of Christensen et al. were obtained in H_2SO_4 liquid-electrolyte cells, whereas our results reflect actual fuel-cell operating conditions. Table 1 shows the kinetic parameters obtained from the *iR*-corrected fuel cell polarization data in comparison to standard Pt electrode. Note also that Tafel

Table 1. Kinetic parameters of polarization measurements reported in Figure 9a and b.

Electrode	Tafel slope [mV dec^{-1}]	E^o [mV]	$I_o \times 10^{3[a]}$ [mA cm^{-2}]	i at 0.8 V [mA cm^{-2}]	i at 0.7 V [mA cm^{-2}]	E at 10 mA cm^{-2} [mV]	Power density at 0.6 V [mW cm^{-2}]
30%Pt/C	72.8	1038	15.9	310	920	949	806
Se/(Ru–Mo)/C	139.8	997	59.0	23	88	821	118
Se/Ru	118.1	963	18.0	–	30	762	45
Ru_xSe_y	146.9	943	29.1	4	38	771	56

[a] Equilibrium exchange current density.

slopes of ca. 70 mV dec^{-1} are in accordance with the literature.[30]

Fuel-cell data were obtained with no overpotential contribution from the hydrogen electrode. Therefore, the overpotentials at the operating current density of 10 mA cm^{-2} shown in Table 1 directly indicate the kinetic limitations of the ORR on the cathode in fuel-cell configuration.

Conclusions

Se/Ru and Se/(Ru–Mo) crystalline carbon-supported nano-electrocatalysts were prepared using the aqueous chemical reduction method. Detailed structural and compositional analyses were performed on the as-prepared and heat-treated materials, where heat treatments resulted in grain growth. The addition of small amounts (about 3 at%) of Mo improved the stability of the electrocatalysts under potential-cycling conditions in O_2-saturated 0.1 M H_2SO_4 solutions. Fuel-cell polarization measurements for Se/(Ru–Mo)/C also showed better performance than for the Se/Ru/C catalysts. The addition of Mo in Ru chalcogenide materials for ORR electrocatalysis is promising because it increases both their stability and their performance.

Experimental Section

Synthesis of Se/Ru/C and Se/(Ru–Mo)/C

The catalyst materials were prepared by chemical reduction of the appropriate salts using the aqueous route previously reported by Campbell.[19] Details of the synthesis procedures have been reported elsewhere;[31] herein, the key steps are briefly described. A carbon suspension was obtained by sonicating 50 mg of Black Pearls 2000 (Cabot Corp.) in 100 mL Millipore water for 1 h, after which time about 160 mg of $RuCl_3{\cdot}xH_2O$ (ca. 10 wt% H_2O, Aldrich Chem. Co.) and 49 mg SeO_2 (99.999%, Johnson–Matthey Co.) were added. The resulting suspension was heated at 80 °C under constant stirring and bubbling of argon for 1 h. After cooling to room temperature, a reducing agent, prepared by dissolving about 95 mg of $NaBH_4$ (98%, Aldrich Chem. Co.) and 200 mg of NaOH (99.998%, Aldrich Chem. Co.) in 25 mL of Millipore water, was added dropwise over a period of approximately 2 h while sonicating the suspension. After the reduction process, the catalyst material was filtered, washed several times with pure H_2O, and dried in air overnight. For the synthesis of Se/(Ru–Mo)/C, about 54 mg phosphomolybdic acid (SPI-Chem) was added to the suspension at the beginning of the synthesis. The mass fractions of Ru in Se/Ru/C and Se/(Ru–Mo)/C catalysts were 45% and 37%, respectively. The mole ratio of Ru to Se was about 1.6 for the two materials and the mole ratio of Ru to Mo in Se/(Ru–Mo)/C was about 2.0. Heat treatments were performed using a tube furnace and a steady argon flow (10 mL min^{-1}), at 500 °C for 2 h and a heating ramp of 10 °C min^{-1}.

Physical Characterization

Powder XRD diffractograms were recorded (UIUC) using a Panalytical X'pert MRD system with a Cu K_α radiation ($\lambda = 0.15418$ nm). The secondary optics consisted of a parallel-plate collimator, a flat graphite monochromator, and a proportional detector. Conventional 2θ–θ scans (where 2θ is the Bragg angle) were recorded with 0.1° steps and 15 s per step counting time.

Elemental compositions were determined (UIUC) using X-ray energy dispersive spectroscopy in a scanning transmission electron microscope (VG HB501 TEM) operated at 100 kV and equipped with an Oxford ISIS Si-Li detector with an ultrathin window (UTW). The sample preparation procedure was the same for all TEM examinations. To prevent agglomerations, each catalyst sample (which was in the form of a fine powder) was dispersed with ultrasound in methanol for about 10 min. The nanoparticles were collected onto a thin carbon film supported by a copper grid by dipping into the dispersed solutions. SEM images were acquired (CWRU) using a dual-beam focused ion beam system (Nova, made by FEI). The electron beam diameter was on the order of 5 nm. TEM analyses were made using a 300 kV FEI Tecnai F30 Super-Twin field-emission gun high resolution TEM; an instrument part of the Swagelok Center for Surface Analysis of Materials (SCSAM) at CWRU. It was equipped with a lithium-drifted silicon detector for XEDS measurements. The electron diffraction patterns were recorded using a Philips CM20 conventional transmission electron microscope operated at 200 kV (CWRU).

Electrochemical characterization

Electrochemical measurements were carried out using an RDE in a three-electrode electrochemical cell equipped with a Luggin capillary. The Au disk ($A = 0.07$ cm^2) with the deposited catalyst, a Pt gauze, and Ag/AgCl/NaCl (3.0 M) were used as the working, counter, and reference electrodes, respectively. All potentials are reported versus the reversible hydrogen electrode (RHE). To prepare the catalyst for deposition, a suspension of 2.5 mg mL^{-1} (either Se/Ru/C or Se/(Ru–Mo)/C) in Millipore water was obtained by sonication for 30 min. A 4.2 μL aliquot of the suspension was placed onto the gold RDE surface and dried in air at room temperature for 2 h. After the electrode was voltammetrically "precycled" between 30 mV and 950 mV in a deaerated 0.1 M H_2SO_4 solution (with argon), the ORR measurements were carried out in the O_2-saturated 0.1 M H_2SO_4 solution at a scan rate of 20 mV s^{-1} while the RDE was rotated at 1600 rpm.[17] The electrode potential was controlled via the Autolab PG-STAT100 potentiostat (Eco Chemie) and the data were analyzed using the General Purpose Electrochemical Software (GPES) package.

Fuel Cell Testing

Fuel cell performance curves were measured (Northeastern University) from a single H_2/O_2 fuel cell with a reference electrode incorporated for simultaneous measurements of half-cell potentials. The curves were obtained after conditioning the membrane electrode assemblies (MEA) at cell potentials of 0.4 V (for 2 to 3 h) and 0.7 V (for 2 h), that is, as long as the steady-state current was measured. Typical polarization measurements took 4 to 6 h. The measurements were carried out at 80 °C and at 0.4 MPa pressure for both the H_2 and O_2 (air) sides. Tests were performed with Se/(Ru–Mo)/C and Se/Ru/C; a commercial Pt/C catalyst (30 wt% Pt on carbon, BASF fuel cells, Somerset, NJ) was also used for comparison. The loading was 0.5 mg cm^{-2} of Ru, and the electrodes were prepared "in-house" using the standard spray methodology, with the catalyst deposited on a commercial gas-diffusion layer (GDL) obtained from BASF fuel cells (LT-1400/W). Details of the electrode fabrication and fuel cell tests are described elsewhere.[32] The anode was a platinized commercial gas-diffusion electrode of 30% Pt/C (0.5 $mg_{Pt/C}$). The cathode electrode loading was also kept at 0.5 mg cm^{-2}. MEAs

were prepared by hot-pressing at 6.9 MPa and 130 °C for 4 min. All polarization measurements were taken under steady-state conditions using a constant-current source, an in-house computer program using LabView package (National Instruments), and the electronic load module from an Agilent instrument (model HP 6050 A). Data were logged when a steady-state potential was reached within the range of ±2 mV. No significant difference between the forward and reverse scans was observed. Under these conditions, the measured hysteresis was within 25 mV. For consistency, only the anodic scan is reported. As mentioned above, the half-cell data were measured using a built-in hydrogen reference electrode at the anode side. This allowed us to measure the variations in the anode electrode overpotentials between various single cell experiments. All measurements showed negligible variations in the anode polarization; thus, the data shown in the polarization and in the Tafel curves represent the cathode polarization only.

Acknowledgements

The authors acknowledge the Army Research Office support through a MURI grant (DAAD19–03–1–0169) for fuel-cell research to Case Western Reserve University and a grant from the US Department of Energy, Office of Hydrogen, Fuel Cells & Infrastructure Technologies (for P.K.B.). XRD, TEM, and XEDS analyses at UIUC were carried out in the Frederick Seitz Materials Research Laboratory Central Facilities, University of Illinois, which is partially supported by the US Department of Energy under grants DE-FG02–07ER46453 and DE-FG02–07ER46471. A.B. would like to acknowledge the National Science and Engineering Research Council of Canada for a post-doctoral fellowship.

Keywords: electrochemistry · nanoparticles · reduction · ruthenium · supported catalysts

[1] R. Dillon, S. Srinivasan, A. S. Arico, V. Antonucci, *J. Power Sources* **2004**, *127*, 112.
[2] H. S. Liu, C. J. Song, L. Zhang, J. J. Zhang, H. J. Wang, D. P. Wilkinson, *J. Power Sources* **2006**, *155*, 95.
[3] J. Y. Park, M. A. Scibioh, S. K. Kim, H. J. Kim, I. H. Oh, T. G. Lee, H. Y. Ha, *Int. J. Hydrogen Energy* **2009**, *34*, 2043.
[4] S. Wasmus, A. Kuver, *J. Electroanal. Chem.* **1999**, *461*, 14.
[5] C. Y. Du, T. S. Zhao, W. W. Yang, *Electrochim. Acta* **2007**, *52*, 5266.
[6] X. Zhang, L. P. Filho, C. Torras, R. Garcia-Valls, *J. Power Sources* **2005**, *145*, 223.
[7] S. C. Thomas, X. M. Ren, S. Gottesfeld, P. Zelenay, *Electrochim. Acta* **2002**, *47*, 3741.
[8] O. Solorza-Feria, K. Ellmer, M. Giersig, N. Alonso-Vante, *Electrochim. Acta* **1994**, *39*, 1647.
[9] T. J. Schmidt, U. A. Paulus, H. A. Gasteiger, N. Alonso-Vante, R. J. Behm, *J. Electrochem. Soc.* **2000**, *147*, 2620.
[10] N. Alonso-Vante, H. Tributsch, O. Solorza-Feria, *Electrochim. Acta* **1995**, *40*, 567.
[11] M. Hilgendorff, K. Diesner, H. Schulenburg, P. Bogdanoff, M. Bron, S. Fiechter, *J. New Mater. Electrochem. Syst.* **2002**, *5*, 71.
[12] A. Kolary-Zurowska, A. Zieleniak, K. Miecznikowski, B. Baranowska, A. Lewera, S. Fiechter, P. Bogdanoff, I. Dorbandt, R. Marassi, P. J. Kulesza, *J. Solid State Electrochem.* **2007**, *11*, 915.
[13] K. Wippermann, B. Richter, K. Klafki, J. Mergel, G. Zehl, I. Dorbandt, P. Bogdanoff, S. Fiechter, S. Kaytakoglu, *J. Appl. Electrochem.* **2007**, *37*, 1399.
[14] R. G. González-Huerta, J. A. Chávez-Carvayar, O. Solorza-Feria, *J. Power Sources* **2006**, *153*, 11.
[15] F. J. Rodríguez, P. J. Sebastian, O. Solorza, R. Perez, *Int. J. Hydrogen Energy* **1998**, *23*, 1031.
[16] H. Tributsch, M. Bron, M. Hilgendorff, I. Dorbandt, V. Eyert, P. Bogdanoff, *J. Appl. Electrochem.* **2001**, *31*, 739.
[17] D. Cao, A. Wieckowski, J. Inukai, N. Alonso-Vante, *J. Electrochem. Soc.* **2006**, *153*, A869.
[18] V. I. Zaikovskii, K. S. Nagabhushana, V. V. Kriventsov, K. N. Loponov, S. V. Cherepanova, R. I. Kvon, H. Bönnemann, D. I. Kochubey, E. R. Savinova, *J. Phys. Chem. B* **2006**, *110*, 6881.
[19] S. A. Campbell, US Patent 7 125 820, **2006**.
[20] S. Fiechter, I. Dorbandt, P. Bogdanoff, G. Zehl, H. Schulenburg, M. Bron, J. Radnik, M. Fieber-Erdmann, *J. Phys. Chem. C* **2007**, *111*, 477.
[21] a) G. Zehl, G. Schmithals, A. Hoell, S. Haas, C. Hartnig, I. Dorbandt, P. Bogdanoff, S. Fiechter, *Angew. Chem.* **2007**, *119*, 7452; b) G. Zehl, G. Schmithals, A. Hoell, S. Haas, C. Hartnig, I. Dorbandt, P. Bogdanoff, S. Fiechter, *Angew. Chem.* **2007**, *119*, 7452; *Angew. Chem. Int. Ed.* **2007**, *46*, 7311.
[22] N. Alonso-Vante, *Fuel Cells* **2006**, *6*, 182.
[23] N. Alonso-Vante, I. V. Malakhov, S. G. Nikitenko, E. R. Savinova, D. I. Kochubey, *Electrochim. Acta* **2002**, *47*, 3807.
[24] J. Zhang, K. Sasaki, E. Sutter, R. R. Adzic, *Science* **2007**, *315*, 220.
[25] V. R. Stamenkovic, B. Simon Mun, G. Wang, P. N. Ross, A. Lucas, N. M. Markovic, *Science* **2007**, *315*, 493.
[26] P. K. Babu, A. Lewera, J. H. Chung, R. Hunger, W. Jaegermann, N. Alonso-Vante, A. Wieckowski, E. Oldfield, *J. Am. Chem. Soc.* **2007**, *129*, 15140.
[27] R. W. Reeve, P. A. Christensen, A. J. Dickinson, A. Hamnett, K. Scott, *Electrochim. Acta* **2000**, *45*, 4237.
[28] K. Suarez-Alcantara, A. Rodriguez-Castellanos, R. Dante, O. Solorza-Feria, *J. Power Sources* **2006**, *157*, 114.
[29] R. G. Gonzalez-Huerta, J. A. Chavez-Carvayar, O. Solorza-Feria, *J. Power Sources* **2006**, *153*, 11.
[30] S. Mukerjee, S. Srinivasan, *J. Electroanal. Chem.* **1993**, *357*, 201.
[31] C. Delacôte, A. Bonakdarpour, C. M. Johnston, P. Zelenay, A. Wieckowski, *Faraday Discuss.* **2009**, *140*, 269.
[32] R. C. Urian, A. F. Gulla, S. Mukerjee, *J. Electroanal. Chem.* **2003**, *554*, 307.

Received: October 29, 2008
Published online on June 24, 2009

